Iranian Journal of Materials Forming 8 (3) (2021) 18-25

Online ISSN: 2383-0042

IJMF

Iranian Journal of Materials Forming

Journal Homepage: http://ijmf.shirazu.ac.ir

Research Article

Textural Evolution of 6061 Aluminum Alloy Processed by Accumulative Roll-Bonding Process

M.R. Rezaei[1,2], M.R. Toroghinejad[1*], F. Ashrafizadeh[1], H. Asgari[3] and J. Szpunar[3]

[1] Department of Materials Engineering, Isfahan University of Technology, Isfahan 84156-83111, Iran
[2] School of Engineering, Damghan University, Damghan, Iran
[3] Department of Mechanical Engineering, University of Saskatchewan, Saskatoon, SK S7N 5A9, Canada

ARTICLE INFO

Article history:

Received 28 February 2021
Reviewed 2 March 2021
Revised 14 April 2021
Accepted 31 May 2021

Keywords:

Al (and alloys)
Accumulative roll bonding
Texture
X-ray diffraction (XRD)

ABSTRACT

A commercial Al-Mg-Si alloy (AA 6061) was deformed by using the accumulative roll bonding (ARB) process for up to five cycles at ambient temperature. The evolution of texture in this process was studied by the X-ray diffraction (XRD) method. Experimental results indicate that the combination of the shear texture composed of Rotated cube {001}<110> component and the rolling textures that included Copper {112}<111> and Dillamore {4, 4, 11}<11, 11, 8> components developed after the first cycle. During the first cycle, the shear texture was developed as a result of shear deformation induced by high level of friction between the rolls and the sheet. By increasing the number of cycles, the shear texture strength diminished and changed to the rolling texture. After the fifth cycle, a remarkable increase in the rolling texture intensity was observed due to homogenous deformation induced by the presence of fine non-shearable particles. Additionally, the presence of magnesium in solid solution influenced the texture evolution during ARB.

1. Introduction

It is well established that the severe plastic deformation (SPD) processes can be used to fabricate a sub-micron/nano-grain structure in various kinds of metals and alloys [1]. The SPD process induces a large deformation strain below the recrystallization temperature [2]. To date, various SPD processes, such as accumulative roll bonding (ARB), equal-channel angular pressing (ECAP), and high-pressure torsion (HPT) have been developed [3]. The ARB process, developed by Saito et al. [4], can impose severe plastic strain on materials and produce sub-micron grains without changing the specimen dimensions [5]. In the accumulative roll-bonding process the rolled material is cut, the surfaces to be joined are roughened and cleaned, and the two parts are stacked and rolled again. By repeating this procedure, very high strains are accumulated in the material, making significant grain refinements possible [6].

It has been shown that the evolution of texture during the ARB process is different from that in conventionally rolled metals [7] because the process is more complex [8]. In the ARB, a large amount of redundant shear strain is introduced in the surface region due to the large friction between the rolls and

* Corresponding author
E-mail address: toroghi@cc.iut.ac.ir (M.R. Toroghinejad)
https://doi.org/10.22099/ijmf.2021.39914.1177

the materials rolled [9]. Additionally, half of the severely deformed regions near the surface is placed in the center in the next ARB cycle. As this procedure is repeated during the ARB process, the redundant shear strain distribution through thickness of the sheet becomes very complicated. The ARB process also leads to accumulated sheets so that the ARB-processed materials contain several interfacial layers parallel to the sheet surface [9]. Skrotzki et al. [10] evaluated textural evolution of an AA6016 aluminum alloy after applying different ARB cycles. The texture after 8 ARB cycles is characterized by the β-fiber with the Cu component dominating. Su et al. [6] found that the bulk texture at the center of 6061 strips shows a gradual increase, up to 5 cycles, in the volume fraction of the Rotated Cube component. In addition, Naseri et al. [11] investigated the texture evolution of commercial purity aluminum (AA1050) after different ARB cycles. They found that the major texture components for ARB specimens are Brass {011}<211> and S {123}<634>. In the other research, special frames were used by McBride et al. [12] to reduce edge cracking and maintain thickness homogeneity during ARB.

The purpose of this study is to investigate, a rather complex, texture evolution in the AA6061 alloy sheet during the ARB process. Microstructural features such as magnesium in the solid solution and non-shearable precipitates in the annealed state can influence textural transformation during ARB.

2. Experimental Procedure

2.1. Sample preparation

The material used in this study was an annealed sheet of 6061 aluminum alloy. The chemical composition of this alloy is shown in Table 1.

Table 1. Chemical composition of 6061 aluminum alloy (wt.%).

Al	Mg	Si	Fe	Cu	Mn	Others
97.30	1.16	0.63	0.49	0.25	0.10	0.07

For the ARB processing, 1 mm thick aluminum alloy sheets were cut into dimensions of 200 mm × 40 mm. The surfaces of the sheets were degreased with acetone and were wire-brushed, to get good bonding prior to roll bonding. The two sheets were stacked together with copper wires such that the brushed surfaces brought into contact and fixed tightly to each other. The roll bonding was conducted at ambient temperature under a dry condition without any lubricant; the reduction in the thickness per cycle was 50 pct, using a rolling mill. The roll diameter was 125 mm and the roll peripheral speed was about 2 m/min. The procedures mentioned here were repeated 5 times, which corresponded to a total equivalent strain of 4.0. Fig. 1 illustrates the procedure.

The microstructure of the material before ARB was observed on the RD-TD plane using a Philips CM12 transmission electron microscope (TEM) operating at 120 kV. Thin foil samples were prepared by twin-jet electropolishing in a A2 Struers solution containing 72 ml ethanol, 20 ml 2–butoxyethanol, and 8 ml perchloric acid (71% concentration) at -3°C. The voltage used for electropolishing was 35 V.

2.2. Texture measurement

Texture measurements were done on the RD-TD section. The specimens have an area of 25 × 15 mm^2 with a flat surface and the subsurface region (one fourth thickness of the sheets) was exposed to the X-ray beam. The samples were prepared by standard metallographic procedures (grinding and mechanical polishing). Texture was recorded using pole figures of (111), (200)

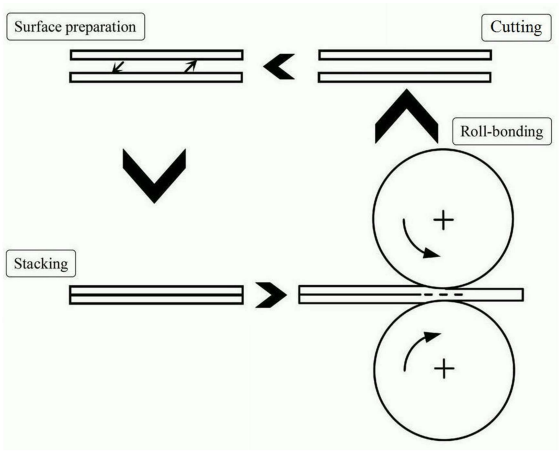

Fig. 1. Schematic illustration of the ARB process.

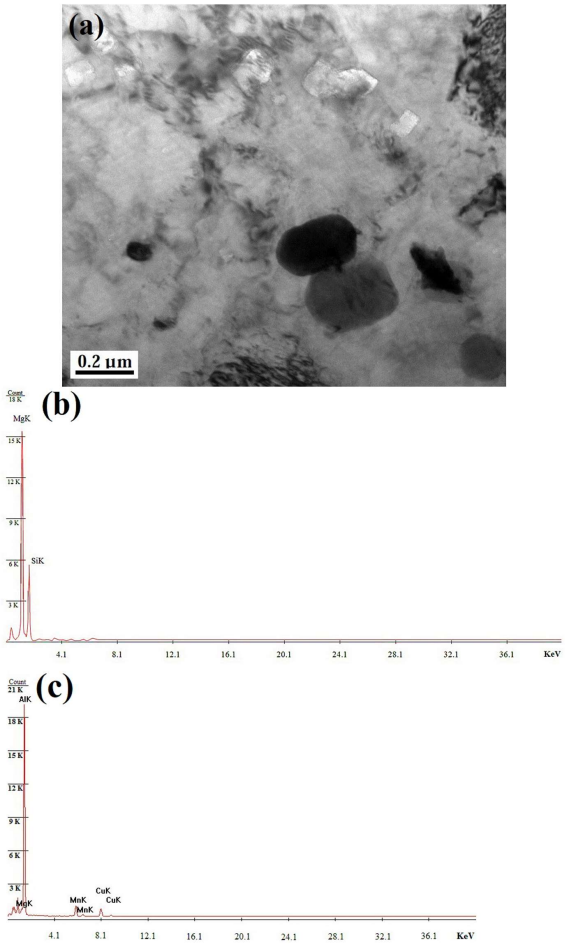

Fig. 2. (a) TEM micrograph of the AA6061 sheet before the ARB process (in annealed state) and EDS analysis of (b) gray particles and (c) black particles.

and (220) planes by X-ray diffraction. The Textools software was used to calculate orientation distribution function (ODF) from the experimental pole figures. In each case, three pole figures were used to determine the ODF. For a better understanding of the texture evolution, the main FCC fibers were calculated from the calculated ODFs.

3. Results

3.1. Initial microstructure

Fig. 2 shows the microstructure as well as the EDS analyses of the annealed AA6061 aluminum alloy sheet prior to the ARB process. Three kinds of particles can be identified in the TEM micrograph: some were white, some gray and some black. White, gray and black particles, which were analyzed by energy dispersive spectroscopy (EDS), are identified respectively as Si-rich, Mg_2Si and Al_6Mn precipitates. The size of the Si rich particles is smaller than that of the Mg_2Si and Al_6Mn precipitates. The average size of each particle is shown in Table 2.

Table 2. The average size of three kinds of particles in the AA6061 Sheet

Average size of particles (nm)		
Gray particle	Black particle	White particle
155	140	95

3.2. Texture evolution during ARB

The {111} pole figures of the ARB processed samples are presented in Fig. 3. All the pole figures are symmetric along RD and TD. Fig. 3(a) illustrates the pole figure of the annealed AA6061 sheet. The main texture component of the annealed sheet is the Cube {001}<100>. After one cycle of ARB, the rolling texture components including Copper {112}<111> and Dillamore {4, 4, 11}<11, 11, 8> are observed (Fig. 3(b)). Fig. 3(c) presents the pole figure of the ARB processed sample after three cycles. The major components are the same as for one-cycle ARB-processed sample, with the difference that their maximum intensity has slightly increased. After the fifth cycle (Fig. 3(d)), the Rotated cube component {001}<110> disappears and the intensity of Copper, S {123}<634>, Brass {011}<211> and Dillamore components increased.

ODFs were calculated from the pole figures and are presented in Fig. 4. Fig. 4(a) illustrates the complete ODF for the annealed sample whose prominent component is Cube. Fig. 4(b) presents the ODF after the first cycle. The textural components can be characterized as the S component, Copper component and Rotated cube component (a typical shear texture component) as well as Dillamore component. In this sample, the Dillamore/Rotated cube component at the $\varphi 1$, φ, $\varphi 2$ =90°,15°,45° with an intensity of 3.5×R (random) is dominant while other components have intensities below 3×R. The three-cycle ARB-processed

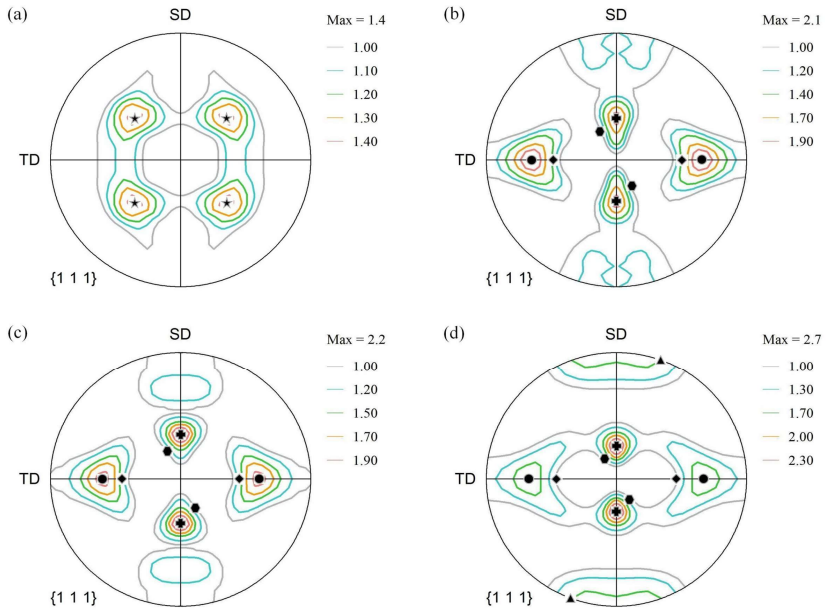

Fig. 3. {111} pole figures: (a) of the annealed sample, (b) after one ARB cycle, (c) after three ARB cycles, and (d) after five ARB cycles. Cube (★) , Copper (✚), Dillamore (●), Rotated cube (◆), Brass (⬢), S (▲).

AA6061 sheet (Fig. 4(c)) shows the textural features are similar to that of the first cycle, however the intensity of the rolling components is higher and the Rotated cube component is lower.

After the fifth cycle (Fig. 4(d)), the intensity of Dillamore, Copper, S and Brass components increased while the intensity of Rotated cube and Dillamore/Rotated cube components reduced. In this state, Dillamore is the major component with the intensity of 5×R.

The textural evolution can also be elucidated using the fibers. The orientation density (f (g)) of fibers was plotted and presented in Fig. 5. The α-fiber is illustrated in Fig. 5(a). It can be seen that there is a nearly homogenous fiber at the initial stage. For ARB processed samples, textural evolution is concentrated mainly around the Brass component and most textural evolutions have occurred around this component. The intensity of the Brass component increases by increasing the number of ARB cycles. Fig. 5(b) presents β-fiber evolution for different ARB cycles. It shows that for the annealed and one cycle ARB-processed samples, the overall intensity of the β-fiber is nearly homogeneous and has a low value. After the third cycle onwards, the overall intensity along Copper to S and S to Brass positions increases gradually. The intensity of the S component remains at the same level during the course of the ARB process. After the final cycle, there was an increase in the level of the β-fiber for all orientations and the prominent component in this fiber is Copper type with intensity of 4×R.

The τ-fiber evolution presented in Fig. 5(c) shows that the textural evolution in the first and third cycle is centered mainly around the Dillamore/Rotated cube component and the intensity of this component increases from 3.5×R after one cycle to 4.5×R after 3 cycles. After the fifth cycle, the intensity of the Rotated cube component is reduced, and the Dillamore/Rotated cube component disappeared. Meanwhile, in the 5 ARB cycles, the maximum intensity of the τ-fiber is at φ= 27°, which coincides with the Dillamore orientation.

4. Discussion

In the present investigation, it is observed that the Cube component is developed in the annealed state (0 cycle sample). During ARB, a texture typical for rolling of face-centered cubic (FCC) metals with high-stacking fault energy develops (Figs. 3, 4). This texture

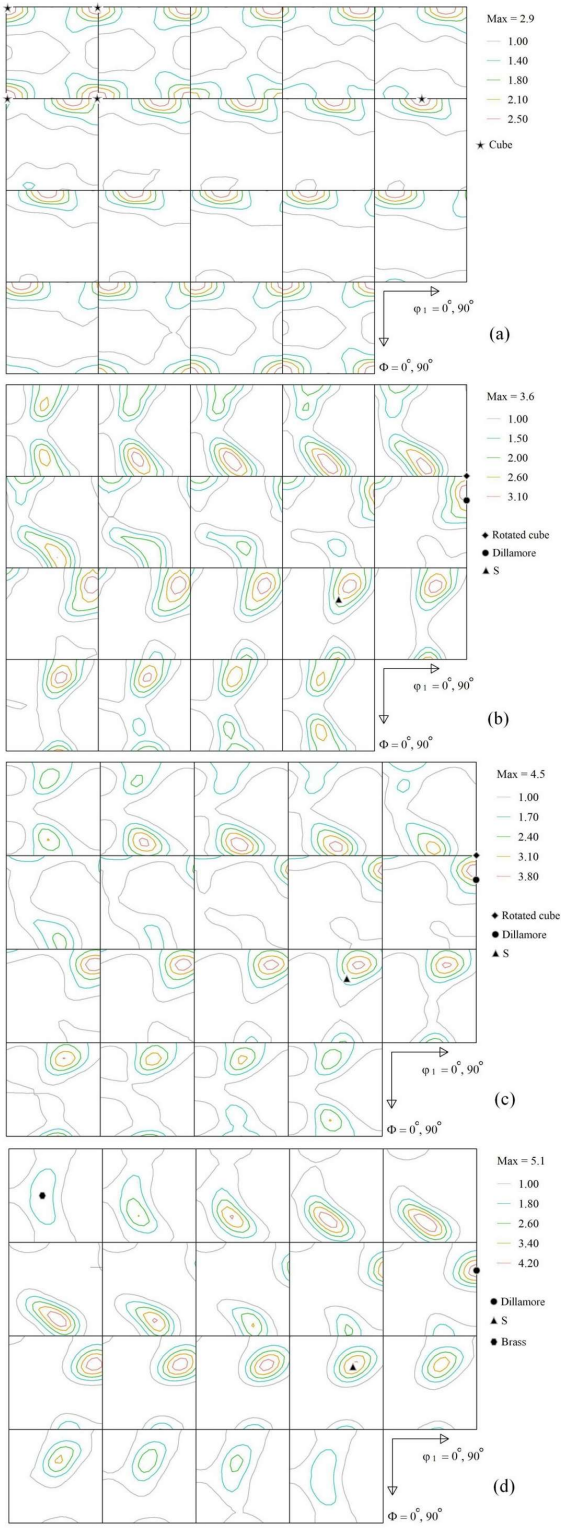

Fig. 4. ODFs (a) of the annealed sample, (b) after one ARB cycle, (c) after three ARB cycles, (d) after five ARB cycles.

is characterized by the β-fiber with the Copper component dominating [13, 14]. Previous authors have shown in their investigation of the textural evolution in aluminum alloys that the intensity of Copper and Goss component increased continuously by increasing the number of ARB cycles, while the intensity of S and Brass components remained unchanged (or reduced) [15, 16]. But, in this study, according to texture evolutions along α and β-fibers (Figs. 5(a) and (b)), the intensity of S and Brass components increase when increasing the number of ARB cycles particularly after the fifth cycle. In materials which have low stacking fault energy, such as Brass, the mechanical twinning on {111}<112> accompanies slip during rolling and this leads to the formation of α-fiber. In these materials, by increasing the strain, the intensity of α-fiber and Brass component increased [5, 17]. It has been reported that presence of magnesium in aluminum solid solution resulted in a noticeable decrease of the stacking fault energy [18, 19], and the Brass texture component is developed during rolling deformation with no mechanical twinning and the shear bands were also not recorded [20]. Hence, the simultaneous increase of Brass and Copper components intensity during ARB (Fig. 5(b)) can be related to the presence of magnesium in 6061 aluminum alloy. During the initial cycles (the first and third cycles), the Rotated cube (shear) component has been seen in ODFs with high intensity. The presence of this component leads to the formation of texture placed between Dillamore and Rotated cube components (Fig. 5(c)). Such a shear type texture forms as a result of redundant shear deformation near the surface during the rolling process. As it was stated earlier, the ARB process has often been carried under dry-surface condition without any lubrication (such as this study). In such cases, a large amount of redundant shear strain is introduced into the surface layers of the rolled sheet owing to a high friction between the sheet surface and the rolls. The formation of the shear texture component in the initial cycles results from introducing shear strain during ARB process.

In the ARB process, one of the sheet surface layers enters the sheet center in the next cycle and then goes up to the quarter thickness in the following cycle. It is different from conventional rolling in which the sheared

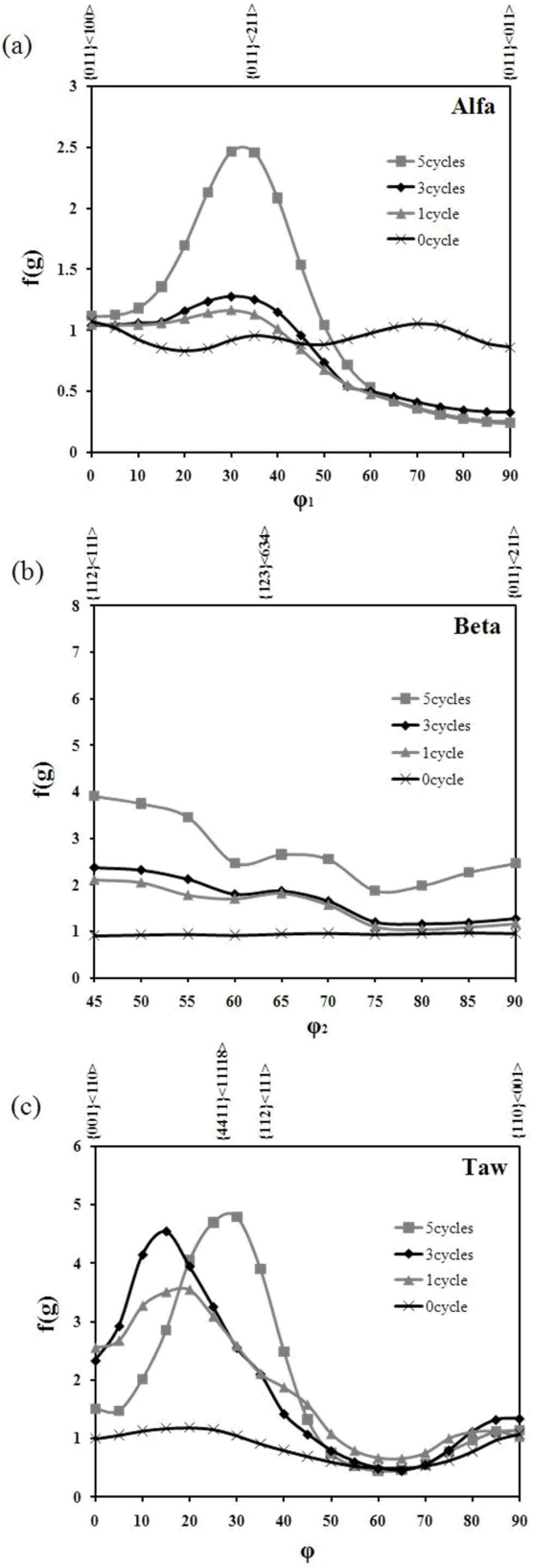

Fig. 5. Developed Fibers during ARB processing of 6061 aluminum alloy: (a) α- fiber; (b) β-fiber and (c) τ-fiber.

regions localize only at subsurface layers and are not distributed throughout the thickness of the sheets.

As mentioned in section 2.2, texture measurements were conducted in the subsurface region (one fourth thickness of the sheets). Thus, the combination of rolling and shear texture components was formed after the first cycle. The destruction of near shear components takes place by increasing number of cycles. Therefore, the shear texture components developed during the first cycle rotation towards the ideal rolling texture components.

After the fifth cycle the intensity of shear component (Rotated cube) is reduced, and the main texture component was Dillamore (Fig. 5(c)). Additionally, as it can be seen in Fig. 5(b), the intensity of S component increased after the fifth cycle. This indicates that due to the additional strain arising from conventional cold rolling (especially after the third cycle).

As stated earlier, the non-deformable particles are associated with a zone of lattice rotation, and in these regions the formation of the normal deformation texture is disrupted [21]. Previous authors have found that the materials containing small non-shearable particles show a sharpening of texture at high strain. The formation of Copper orientation was fully described using the fully constrains model (Taylor model) [9]. This is expected to result from reduction in the mean free path of dislocations movement related to the presence of particles. In the ARB-processed AA6061 sheet, the ultrafine grain size and the fine non-shearable particles led to a rather homogeneous Taylor-like deformation (polyslip), which consequently enhanced probability of the stable orientation. The results suggested that either the sub-micron grain formation, the fine precipitates, or both, had a significant role in strengthening the Dillamore texture, after 5 ARB cycles.

The low strength of texture, up to five cycles, can be explained by the formation of deformation zones near second-phase particles [9, 20]. Because the AA6061 alloy sheet before the ARB contains a large number of second-phase particles (Fig. 2), a large number of deformation zones were introduced in the Al matrix during the ARB process, which weakened the rolling texture.

4. Conclusions

In this study, the ARB process was repeated up to five cycles at ambient temperatures on AA6061 sheets. The texture of the samples was evaluated after each cycle. The conclusions can be summarized as follows:

1. The developed texture during this process showed the rolling symmetry for all cycles.

2. After the first cycle, the combination of shear and rolling texture components involving Copper, Rotated cube and Dillamore/Rotated cube components was formed. Formation of the shear component is related to shear deformation near the surface during rolling.

3. After three cycles, the overall texture intensity increased slightly, except for the Rotated cube component, because the shear texture developed in the previous ARB cycle was destroyed and transformed into the rolling texture.

4. A decrease in the intensity of the shear texture was observed after five cycles. In addition, the intensity of the rolling texture, especially the Dillamore orientation, increased. A sharp increase in the Dillamore orientation was caused due to the rotation of shear texture component to the rolling texture components and homogenous deformation induced by fine non-shearable particles present in the microstructure.

5. References

[1] M. R. Rezaei, S. G. Shabestari, S. H. Razavi, Investigation on equal-channel angular pressing-induced grain refinement in an aluminum matrix composite reinforced with Al-Cu-Ti metallic glass particles, *Journal of Materials Engineering and Performance*, 28(5) (2019), 3031-3040.

[2] Y. Cao, S. Ni, X. Liao, M. Song, Y. Zhu, Structural evolutions of metallic materials processed by severe plastic deformation, *Materials Science and Engineering: R: Reports*, 133 (2018) 1-59.

[3] N. Tsuji, Y. Saito, S. H. Le, Y. Minamino, ARB (Accumulative Roll-Bonding) and other new techniques to produce bulk ultrafine grained materials, *Advanced Engineering Materials*, 5(5) (2003) 338-344.

[4] Y. Saito, H. Utsunomiya, N. Tsuj, T. Sakai, *Novel ultra-high straining process for bulk materials—development of the accumulative roll-bonding (ARB) process*, Acta Materialia, 47(2) (1999) 579–583.

[5] M. Rae, M. R. Toroghinejad, R. Jamaati, J. Szpunar, Effect of ARB process on textural evolution of AA1100 aluminum alloy, *Materials Science and Engineering: A*, 527(26) (2010) 7068-7707.

[6] L. Su, C. Lu, A. A. Gazder, A. A. Saleh, G. Deng, K. Tieu, H. Li, Shear texture gradient in AA6061 aluminum alloy processed by accumulative roll bonding with high roll roughness, *Journal of alloys and compounds*, 594 (2014) 12-22.

[7] M. Shaarbaf, M.R. Toroghinejad, Evaluation of texture and grain size of nanograined copper produced by the accumulative roll bonding process, *Metallurgical and Materials Transactions A*, 40(7) (2009) 1693-1700.

[8] H.W. Kim, S.B Kang, Z.P. Xing, N. Tsuji, Y. Minamino, Deformation textures of AA8011 aluminum alloy sheets severely deformed by accumulative roll bonding, *Metallurgical and Materials Transactions A*, 36(11) (2005) 3151-3163.

[9] P. Chekhonin, B. Beausir, J. Scharnweber, C. G. Oertel, T. Hausöl, H. W. Höppel, H. Brokmeier, W. Skrotzki, Confined recrystallization of high-purity aluminium during accumulative roll bonding of aluminium laminates, *Acta Materialia*, 60(11) (2012) 4661–4671.

[10] W. Skrotzki, I. Hünsche, J. Hüttenrauch, C.G. Oertel, H. G. Brokmeier, H. W. Höppel, Texture and mechanical anisotropy of ultrafine-grained aluminum alloy AA6016 produced by accumulative roll bonding, *Texture, Stress, and Microstructure*, 2008.

[11] M. Naseri, M. Reihanian, E. Borhani, Effect of strain path on microstructure, deformation texture and mechanical properties of nano/ultrafine grained AA1050 processed by accumulative roll bonding (ARB), *Materials Science and Engineering: A*, 673 (2016) 288-298.

[12] B. N. McBride, K. D. Clarke, A. J. Clarke, Mitigation of edge cracking during accumulative roll bonding (ARB) of aluminum strips, *Journal of Manufacturing Processes*, 55 (2020) 236-239.

[13] R. Jamaati, M. R. Toroghinejad, Effect of stacking fault energy on deformation texture development of nanostructured materials produced by the ARB process, *Materials Science and Engineering: A*, 598 (2014) 263-276.

[14] W. Liu, X. Kong, M. Chen, J. Li, H. Yuan, Q. Yang, Texture development in a pseudo cross-rolled AA 3105 aluminum alloy, *Materials Science and Engineering: A*, 516(1-2) (2009) 263-269.

[15] H. Pirgazi, A. Akbarzadeh, R. Petrov, J. Sidor, L. Kestens, Texture evolution of AA3003 aluminum alloy sheet produced by accumulative roll bonding, *Materials Science and Engineering: A*, 492(1-2) (2008) 110–117.

[16] O. A. Velázquez-Carrillo, F. A. García-Pastor, Thermal stability of microstructure, mechanical properties,

formability parameters and crystallographic texture in an Al-7075 alloy processed by accumulative roll bonding, *Journal of Materials Research and Technology*, 11 (2021) 2208-2220.

[17] H. R. Wenk, P. Van Houtte, Texture and anisotropy, *Reports on Progress in Physics*, 67(8) (2004) 1367-1428.

[18] P. Snopiński, M. Król, Microstructure, mechanical properties and strengthening mechanism analysis in an AlMg5 aluminium alloy processed by ECAP and subsequent ageing, *Metals*, 8(11) (2018) 1-14.

[19] G. Nurislamova, X. Sauvage, M. Murashkin, R. Islamgaliev, R. Valiev, Nanostructure and related mechanical properties of an Al–Mg–Si alloy processed by severe plastic deformation, *Philosophical Magazine Letters*. 88(6) (2008) 459-466.

[20] T. Leffers, R. K Ray, The brass-type texture and its deviation from the copper-type texture, *Progress in Materials Science*, 54(3) (2009) 351-396.

[21] F. J. Humphreys, M. Hatherly: Recrystallization and Related Annealing Phenomena, Elsevier Science Ltd., Oxford, United Kingdom, 2004, pp.1205-1209.